

1

1 **Mobilization of geochemical elements in the active layer of**
2 **permafrost to surface water in Russian Arctic**

3

4 **Xiaowen Ji^{a,b,c}, Evgeny Abakumov^b, Vyacheslav Polyakov^{b,d,e}, Xianchuan Xie^{a*}**

5

6 ^a *State Key Laboratory of Pollution Control and Resource Reuse, School of the Environment,*
7 *Nanjing University, Nanjing, 210093, P. R. China*

8 ^b *Department of Applied Ecology, Saint Petersburg State University, Saint Petersburg,*
9 *199178, Russian Federation*

10 ^c *School of Environment and Sustainability, University of Saskatchewan, Saskatoon SK, S7N*
11 *5B3, Canada*

12 ^d *Arctic and Antarctic Research Institute, Saint Petersburg, 199397, Russian Federation*

13 ^e *Department of Soil Science and Agrochemistry, Saint-Petersburg State Agrarian University,*
14 *Pushkin, Saint Petersburg, 19660, Russian Federation*

15

16 * Corresponding author's e-mail: xchxie@nju.edu.com

17 **Abstract**

18 The predicted increasing ground temperatures in the Arctic results in the deepening of the active
19 layer and intensification of geochemical processes, which could affect the geochemical
20 composition of surface waters. Determining the responses of the riparian soil systems to
21 surrounding hydrological flows under changing climate conditions is important for understanding
22 the seasonal changes in hydrological processes. Therefore, in this study, one soil core from the
23 study area polygon rim (close to the Taz River, TA) and two soil cores from the riverain terrace
24 (close to the Syoyakha River, SY and Murtyyakha River, MU) in Russian Western Siberia and
25 their supra-permafrost water, adjacent stream flows and river water were sampled for analysis of
26 geochemical elements. The results showed that most elements above their respective detection
27 limits (Mn, Sr, Fe, Mg, Cr, Co, V, Pb, Al and Ca) started to accumulate in the downwards gleyed
28 layer during September–October in response to the deepest thaw in the active layer. This study
29 focused on the highly mobile elements, i.e., Mn, Ca, Mg, Al and Ti, in the deepest layer; and
30 found that the transport of organic matter in the upper layer carried these elements to both surface
31 water ponds/flows and supra-permafrost water, and further, to the rivers. The best linear
32 correlation for both stream flows and river water were Mn, which may be a proxy for predicting
33 the processes occurring within the active layer during the annual summer-autumn thaw. Finally,
34 landscapes with different ice contents may experience changes in the elements transported to
35 surface waters.

36

37 **Keywords:** Geochemical elements, Arctic, Permafrost-affected soils, active layer, surface water,
38 seasonal thawing

39

1. Introduction

The increasing atmospheric temperatures in the Arctic have led to permafrost thawing and vertical downward migration of the active layer into formerly frozen ground, during the thawing season (Christiansen et al. 2010, Connon et al. 2018, Jorgenson et al. 2010, Romanovsky et al. 2010, Smith et al. 2010). The active layer responds to the changing climatic conditions by increasing its depth, thus accelerating chemical weathering (Colombo et al. 2019, Keller et al. 2007, 2010) and potentially releasing geochemical components and organic carbon from the soil to adjacent aquatic landscapes (Barker et al. 2014, Grosse et al. 2016, Johnson et al. 2013, Johnston et al. 2014, Loiko et al. 2017, Raudina et al. 2018, Schuur et al. 2015). This would increase the movement of carbon dioxide (CO₂) from the soil to aquatic reservoirs such as rivers and lakes (Elder et al. 2019, Natali et al. 2015, Polishchuk et al. 2018, Wild et al. 2019); this occurs through the transport of solute and water along surface streams and the permafrost table, which is as known as “supra-permafrost flow”. Supra-permafrost water is found in the shallow subsurface of the active layer, where it is typically situated at the boundary between the frozen and thawed fractions of the soil profile (Cederstrom et al. 1953). Owing to the absence of groundwater discharge in the permafrost-affected region, solutes being transported to lakes or rivers from adjacent soils originate primarily from supra-permafrost water.

Permafrost degradation has been associated with an increased contribution of groundwater to stream via surface flows or supra-permafrost water in Canadian Arctic rivers (Walvoord and Striegl 2007). Ice wedge degradation has also been proven to be related to the water balance of lowland across the Arctic landscapes, and to increase streamflow (Liljedahl et al. 2016). Several studies have observed substantial increments in discharges from the major Eurasian Arctic rivers due to the warming climate (Brown et al. 2019, Feng et al. 2019, Lammers et al. 2001, Yang et al. 2002, Zheng et al. 2019). Raudina et al. (2018) observed a northward shift of the permafrost boundary under climate change scenarios, and that the concentrations of dissolved organic carbon (DOC), major and trace elements, and greenhouse gases are expected to decrease in the supra-permafrost waters at the border between the thawed and frozen parts from peat soils in the western Siberia lowland. Loiko et al. (2017) hypothesized that the direct mobilization of soil waters to

68 hydrological networks and the transformation of autochthonous processes were controlled by
69 physical factors in different landscapes. Overall, there appears to be considerable variability and
70 uncertainty regarding how discharges of DOC, elements, and greenhouse gases in supra-
71 permafrost waters/surface flows respond to permafrost thaw and are released to surface water
72 ponds and rivers.

73 Several studies concerning the biogeochemical cycles of carbon and related metals focused
74 on both the aquatic and the terrestrial parts of the continental permafrost-bearing ecosystem (Guo
75 et al. 2007, McClelland et al. 2007, Olefeldt and Roulet 2012, Pokrovsky et al. 2011). More
76 recently, the biogeochemistry of soil porewater and supra-permafrost water in mineral and
77 organic/peat parts of soil profiles in the permafrost areas have been studied (Barker et al. 2014,
78 Jessen et al. 2014, Lamhonwah et al. 2017, Loiko et al. 2017, Raudina et al. 2018, Street et al.
79 2016). The previous studies concluded that the export fluxes of DOC, greenhouse gases, and trace
80 metals from the active layer of permafrost to the surrounding hydrological landscapes are
81 determined by the amount of water passing through the active layer till the border of the frozen
82 permafrost, before being drained to a lake or river (Pokrovsky et al. 2016a, Pokrovsky et al.
83 2016b, Raudina et al. 2018). Barker et al. (2014) reported that the concentrations of metals in
84 surface water were related to the increasing active layer thickness/degrading permafrost during
85 late fall and early winter. These results revealed that the dynamics of trace metal concentrations in
86 the transitions from Arctic soils to surface water corresponded to top-down freezing processes in
87 the active layer. However, there is a lack of information connecting geochemical tracers in both
88 the underlying supra-permafrost flow and the upper soil layer to explain the transport of
89 geochemical compositions to surrounding hydrological networks and can be used as a proxy for
90 the seasonal active layer dynamics.

91 Therefore, this study aims to provide this knowledge by analyzing supra-permafrost water, soil
92 pore water, surrounding small water ponds/flows, and eventually, river surface water from three
93 typical soils close to rivers from continuous permafrost regions within the Yamal and Gydan
94 peninsulas, West Siberian Arctic. Tundra lakes and river floodplains are abundant in the Yamal and
95 Gydan peninsulas; lakes cover, on average, 10% of the Yamal peninsula, occupying 20% of the
96 floodplains of large rivers (Dvornikov et al. 2019). Approximately 90% of all lakes in the study

region are small ($<1 \text{ km}^2$) water bodies. To analyze the effluxes of permafrost soils from relatively homogeneous landscapes, the sampling sites were set up next to the largest rivers flowing to the Kara sea, such as the Syoyakha, Murtyyakha, and Taz Rivers. Our main working hypotheses are as follows: (i) Based on the response of riverine DOC and element concentrations to increasing active layer thickness reaches the highest contents during late autumn, when the active layer reaches its greatest depth in a year. Besides, when the components' concentrations in the base flow increases, with the yearly maximum values being observed in the Siberian rivers (Yang et al. 2002). Therefore, the dominant contributor of DOC and trace elements to river waters during this time of the year is expected to be supra-permafrost water and base flow to the rivers. (ii) When mineral weathering processes continue in the deeper soil column during late autumn and early winter, shallow subsurface soil can also store major mobilized components, such as DOC, in late autumn during freezing; these components bind with elements and can contribute to spring thaw in the next year. Formerly mobilized components stored in the shallow subsurface during spring snowmelt can be potentially enhanced to supra-permafrost waters and further to surrounding surface waters. Therefore, with an increasing thawed depth of permafrost and the potentially enhanced mineral weathering fluxes into supra-permafrost waters, biogeochemical fluxes from surrounding surface waters may experience a change during spring and autumn. (iii) As the DOC and elements are controlled by the redox environment of riparian soils, they cannot be consumed by the surrounding biota or depleted by abiotic reaction, and thence persist in supra-permafrost water; they may be transported to the surrounding hydrological network.

The specific objectives of this study were (1) to assess the mobility of releasing geochemical elements from upper soil layer water and supra-permafrost water to surrounding water bodies; (2) to examine whether the concentrations of geochemical elements in the surface water (connected streams and received river) can explain the active layer dynamics of permafrost riparian soils in different permafrost-affected landscapes.

123 2. Studying site and methods

124 2.1 Geographical setting

125 The study area was located in the Northwest area of the Yamal-Nets Autonomous Region,
126 across 66° N, with continuous permafrost (**Figure 1A**). Sampling sites were located close to
127 the lowlands of the Syoyakha, Murtyyakha, and Taz rivers. The Syoyakha and Murtyyakha
128 Rivers are situated in the Yamal Peninsula on the Western Siberian plain (Golovatin et al.
129 2011). These geographical features of this region are strongly divided between river valleys,
130 lake hollows, and streams (Golovatin et al. 2011). Cryogenic soils in this part of the Yamal
131 Peninsula were formed due to the high ice content of Holocene alluvial sediments (Sidorchuk
132 and Grigorev 1998) and aeolian materials (Alekseev and Abakumov 2018). This part of the
133 lowland comprises very flat watersheds of the Syoyakha and Murtyyakha Rivers and is
134 covered with frozen bogs and palsa. The Syoyakha is one of the largest rivers of the Yamal
135 Peninsula (Bespalaya et al. 2018); its watercourse is 165 km long and its watershed covers an
136 area of 4,400 km² (Bespalaya et al. 2018). The Murtyyakha River has roughly 580
137 watercourses and numerous lakes in its basin, which contains 70 rivers more than 10 km long.
138 The Murtyyakha River flows into the Syoyakha River and then enters Kara Sea. Syngenetic
139 permafrost close to these two rivers contains massive Holocene ice deposits (Vasil'chuk et al.
140 2016). The 1,401 km long Taz River is located in the Gydan Peninsula and drains a basin of
141 150,000 km²; it flows into the Taz Estuary and ends in the Gulf of Ob. Soils along with the
142 river included alluvial stratified parent deposits from an earlier stage of the Holocene
143 (Tarnocai 2009).

144 We investigated the three poorly drained riparian soils with upper organic layers and a
145 downward mineral profile adjacent to each river (**Figure 1A**). The soil close to the Taz River
146 site (TA) was located at the top of the polygon rim, where the landscape is polygonal tundra,
147 and the center of polygon was wet-depressed and an accumulation of organic matter poorly
148 degraded by anaerobic conditions; the surrounding elevated polygon rim showed the evidence

of cryoturbation in most horizons in the active layer (**Figure 1B**). The soil profile was gleyed with frost heaving of the clay stratum. The surrounding vegetation consists predominantly of wet acidic tussock sedge, grass, and sphagnum moss. Soils sampled nearby at the Syoyakha (SY) and Murtyyakha (MU) Rivers were both situated from the floodplain. The SY site consisted of moist acidic moss, lichen, and sedges, and MU site consisted of lingonberry, willow, moss, and sedge. Both soil profiles had shallow active layers that were strongly gleyed and under reducing conditions, while the deeper layers at MU showed obvious signs of cryoturbation (**Figure 1C and D**). The formation of the SY and MU stratified soils may have resulted from the constant changes in the river water levels. All three soil profiles for TA, SY, and MU have been depicted as relatively light chroma color with oxidation of iron minerals and dominated by mineral substrates with allochthonous organic matter or autochthonous peat.

2.2 Soil core and supra-permafrost water collection and analysis

Three soil cores were extracted up to the permafrost table using a portable Snow-Ice Permafrost-Research-Establishment (SIPRE) auger set consisting of a coring auger and an engine from Jon's Machine Shop, Fairbanks, Alaska, USA. The location of each soil core was directly adjacent to the borehole into which a string thermometer was inserted (**Figure 1A**). The thermometers, which were put in cases filled with grease as an inert material, were placed roughly 10 cm from permafrost table for 24 h in July 2016 in order to reach thermal equilibrium with surrounding soil material. The thermometers were connected to a data logger for recording hourly temperatures in degrees Celsius (Modular GM10, Yokogawa Electric Corporation, Tokyo, Japan), powered by a battery with a three-year life and attached to a stainless-steel stake inserted into the soil cores. The excavated local soils were moved back to the soil cores. The cores were collected in May 2016, sealed with Polyethylene covers, transported at a stable temperature of -4 °C to freeze the soils, and stored in a refrigerator at the same temperature prior to analysis. We believe the cores can partially reflect the deepest active layer during a year, with approximately 65 cm for Mu, 46 cm for Sy, and 90 cm for Ta

shown by the thawing materials. The soil pits were excavated in July 2017 adjacent to the coring location (**Figure 1**), and site restoration procedures followed the standard protocols for permafrost-affected soils (Ping et al. 2013). Excavating soil pits may provide an insight into the vertical depth between the active layer and permafrost that contain external flows to rivers. Each 35 × 35 cm soil pit was excavated with a shovel and hatchet until reaching frozen materials and the genetic horizon and name of each soil were identified using the World Reference Base for Soil Resources WRB (2015) classification system. The stagnic condition of soils meant that we had to use 2,2'-Dipyridyl to spray soils for 30 s to test for reducing conditions, as per the tests previously conducted on gleyed soils (Ping et al. 1998).

The frozen soil core was cut into 5 cm sections with a diamond wire saw (LKH-8, Kanghua Company, Guilin, China), with a cutting section of diamond-impregnated wire mounted on idler pulleys, in a cold room in the laboratory of Arctic Logistics Center, Salekhard, Yamal-Nenets Autonomous Region, Russia. The cut sections of each soil core were then placed in tightly sealed plastic bags (9.5 cm x 18 cm, Bag Whirlpak Clear 7oz, Nasco, FL, US) and kept at room temperature (approximately 23 °C) to thaw for 12 h. Completely thawed soils were used to collect soil porewater with an SPS 200 lysimeter soil solution sampler (SDEC, Reignac-sur-Indre, France). The collected water was filtered through a 0.45 µm polypropylene filter, decanted to glass test tubes, and acidified with 0.5(wt) % ultrapure nitric acid (HNO₃, CAS: 7697-37-2 Fisher Scientific, Hampton, USA) before processing through inductively coupled plasma-tandem mass spectrometry (8800 ICP-MS/MS, Agilent, Santa Clara CA, USA). To remove the spectral interferences of ions through ion/neutral reactions, the collision reaction cells (CRCs) mode in the ICP-MS was operated using He or NH₃ as the inert collision gas, following the protocol developed by McCurdy and Woods (2004). The elements V, Cr, Mn, Fe, Co, Ni, Cu, Zn, and As were analyzed in CRCs mode with He gas to remove unidentified polyatomic particles arising from the variables Cl⁻, S⁻, and C⁻. Ti was analyzed in CRCs mode with NH₃ to remove interference from S-based polyatomic ions. The elements Sr, K, Ca, Mg, Al, Ba, Be, B, Cd, Pb, Au, Mo, P, Sc, Ag, Tl, Sn, and rare earth

elements (REEs) were analyzed using normal (non-CRCs) mode.

Four calibration standards (1×10^{-2} , 1×10^{-1} , 1×10^1 , $1 \times 10^2 \mu\text{g L}^{-1}$) were prepared by diluting $1 \times 10^3 \mu\text{g L}^{-1}$ stock standard solution for each element and mixed REEs (TraceCERT®) purchased from Sigma-Aldrich, St. Louis MO USA. The 2% (w/w) ultrapure HNO_3 was taken as the blank. Calibration was performed before every analytical test with a good calibration curve ($R^2 \approx 0.999$), and three blanks and check standards were run before every ten samples. The analytical uncertainty for each sample was determined by the analysis of triplicate within an error of $\pm 3\%$. The detection limits for all elements were set at the level of $1 \mu\text{g L}^{-1}$. To correct the magnitude of the signal suppression or enhancement, a standard mixture solution of Bi, Ge, In, Li, Sc, Tb, and Y ($10 \mu\text{g /mL}$) prepared in 2% ultrapure HNO_3 was used as the internal standard added in all standards, blanks, and samples.

Then, each soil core section was transported to the Applied Ecological Laboratory, Saint Petersburg State University. They were dried in a vacuum drying oven for 16 h, homogenized by grinding using a roller mill, processed through a 2-mm sieve, and finally, soils were pressed into a powder pellet with a vertical hydraulic jack. Each pellet was analyzed through scanning electron microscopy with energy dispersive X-ray spectroscopy (SEM-EDX) (JSM-6390 LA, EX2300, JEOL, Tokyo, Japan). EDX revealed the characteristic peak for each metal in each sample with atomic-level precision, which can directly transfer the concentration in terms of mg kg^{-1} . The soil certified reference material CRM027 and SQC001-30G (Sigma-Aldrich, St. Louis, USA) for trace metals were used for calibration. Samples and the reference material were analyzed in triplicate, and the detection limits were determined based on the minimum value of the reference material.

The location of stagnant supra-permafrost waters was collected adjacent to the previous soil cores in September 2016. To prevent the contamination of water samples due to the previous methods of collecting supra-permafrost waters with soil pit excavation, an alloy probe rod was first inserted into the soil to confirm approximately the same depth of the active layer–permafrost boundary as the previous soil core. A direct push device (SP16

Groundwater Sampler, Geoprobe Systems®, Salina KS USA) comprising a polyvinyl chloride screen was driven to the permafrost table within a sealed steel sheath. Then, the water samples were pumped through the tube to the surface and stored in 25-mL PVC serum bottles by oscillating the tubing up and down.

For the lower floodplain (SY and MU), water samples were collected after pumping the tube for 15–20 min to flush water with permafrost materials. The time required for pumping water in TA was relatively longer than that for the other sites, by approximately 30 min, with less volume of inflowing water because of the higher depth of polygon rim. For all sites, the first portion of water containing permafrost materials was discarded, and the clearer water with fewer impurities was collected. Unfiltered water Samples in the serum bottles were treated with 0.2 mL of mercuric chloride (HgCl_2 , Sigma-Aldrich) and capped without air bubbles or headspace using butyl rubber stoppers pierced by a needle attached to a 3-mL syringe that allows air and water escape from the bottle when the stopper is inserted. With the bottle inverted, 10 ml of methane-free helium (Sigma-Aldrich) was added, meanwhile 10 ml of water was removed through needle displacement and the syringe. Then, another 10 ml of methane-free helium was added to the headspace without removing water, and water and headspace were equilibrated in the bottle by shaking for 2 min. The triplicates of subsample headspace gas (into the syringe) were analyzed for CH_4 and CO_2 by gas chromatography (GC-456, Bruker, Billerica MA, USA), with flame-ionization detection (FID) and electron capture detection (ECD), respectively. After each set of ten samples, the detectors were calibrated based on Air Liquide ($\text{CO}_2 = 246.6 \mu\text{mole/mole}$, $\text{CH}_4 = 302.3 \mu\text{mole/mole}$). The results of triplicate injection showed a repetition rate within $\pm 2\%$. The gas solubility of CH_4 and CO_2 (Kastanidis et al. 2018) were taken by calculating the total concentration of CH_4 and CO_2 in the vials and then converting to $\mu\text{mol/L}$ of the initial samples. All analysis procedures for analyzing CH_4 and CO_2 were carried out in the Center for Chemical Analysis and Materials Research of St. Petersburg State University. The water temperature, dissolved oxygen, pH, and specific conductivity were field measured with a portable multiparameter meter (Orion

Star™ A329, ThermoFischer Scientific, Waltham MA, USA). Stagnant supra-permafrost waters in this study were oxygenated with an average O₂ saturation in samples ranging from 10.2 to 82.3% with an uncertainty of 3-4%, which is very close to the previous reports in Western Siberian lowlands (Loiko et al. 2017, Raudina et al. 2018). No significant difference was observed in the O₂ concentrations from water samples in each soil site. The average temperature of supra-permafrost waters did not vary significantly as 12.3±1.8 °C for SY, 13.4±1.6 °C for MU, and 15.6±2.0 °C for TA. The dissolved organic carbon (DOC) concentrations were analyzed by a TOC-L TOC Analyzer (Shimadzu Kyoto, Japan) with an uncertainty of 5% and a detection limit of 4 µg/L.

2.3 Surface water collection and analysis

All surface water samples were collected in September 2016. All sampling sites were adjacent to the location of the soil cores. We collected water samples (streams connected to each river) from shallow (< 10-30 cm) permafrost subsidence and hollows with the size of < 1 m²; deep depressions (< 1 m) of palsa bogs with sizes ranging from 5 to 15 m²; small thaw ponds with sizes ranging 10-150 m²; and each river closest to the soil core within 5–10 m (depth < 5 m). Neoprene gloves were used during water sampling, and water from the shoreline was collected by a standard PVC MP² two-stop peristaltic pump tubing (1.09 mm I.D., White/Red, Pkg. 12, PerkinElmer, Waltham MA, USA) outfitted with a pre-sterilized Durapore® 0.45 µm capsule filter (MilliporeSigma, Burlington MA, USA). The water passing through the tubing and filter capsules for the first 30 s was not collected, and polypropylene (PPCO) bottles with white PP closure precleaned by 2% nitric acid were used for water collection. The analysis of trace metals in water samples was the same as in subchapter 2.2. The samples used for chloride determination were not acidified. Chloride determination was performed by titration with silver nitrate (AgNO₃, 0.02 mol L⁻¹) as titrant according to ISO 9297: 2000 “Water quality — Determination of chloride — Silver nitrate titration with chromate indicator (Mohr's method).” Titrant calibration was used by standardizing AgNO₃ solution versus NaCl solution with the same molar concentration (0.02

mol L⁻¹). The relative standard deviation (RSD) of titrant was <1 %.

3. Results

3.1 Characteristics of soil profile and chemical composition in the soil column

The detailed horizon and vegetation information in the soil pit profiles in the photographs for SY, MU, and TA is shown in **Figure 1**. The soil group belongs to Histic Gleysols (Stagnic), Histic Gleysols (Turbic), and Turbic Cryosols for SY, MU, and TA, respectively. The top fractions of soil horizons from three soil pits all show a high chroma color, with TA being relatively lighter (**Figure 1B**), and all the lower fractions show strong gleyed conditions, which may indicate a redox boundary. The lower fractions of soils were further tested by a few drops of alpha-alpha-dipyridyl for 30–40 s, showing that no pink color was observed for SY at the depth of 6–9 cm, with a strip-shaped iron oxidized boundary to the next horizon. A positive pink color was observed during the reaction in the next gray color horizon (9–18 cm), suggesting the occurrence of reduced ferrous oxides under the reducing condition. Compared with the previous horizon, this horizon had few plant roots and little accumulation of organic matter. The lowest section (18–35 cm depth) had a sporadic positive pink color. This difference may be due to the different redox spots visually observed in the excavated soil pit (**Figure 1C**). The lower 18–35 cm showed heterogeneous rusty-gray color as the ferric irons, as well as aluminum, and inclusions of organic materials due to the cryogenic mass exchange through bottom-up transportation of water by thawing/freezing processes that bring parent materials to the upper layers, where cracks can be observed in 18–35 cm. In the upper 6–9 cm horizon, the oxidation of ferrous iron to ferric iron is mostly due to the leaching process of upper thawing water containing oxygen. Therefore, the low density of strictly reduced gleyed horizon (6–9 cm) separated the two different geochemical transport pathways between the upper and lower horizons.

For soil pit MU, the pink reaction color was observed at the depth of 7–25 cm (the shape shown as B_{g@} horizon in **Figure 1D**), and the middle part of depth 25–60 cm and 60–65 cm

depth. In the B_{g@} horizon, there were more disbursed rust-orange spots and stains that followed the path of roots; these ferrous irons were oxidized by the atmosphere through the growth upper vegetation's roots growing. In the 25–60 cm depth, the apparent presence of cryoturbation with a gray-brown color was observed alongside the dark-gray inclusions from the lower permafrost. The oxidized iron in this horizon results from the multi-year freezing/thawing and lower activities of congeliturbation that transport the materials from both the upper and lower layers. The 60–65 cm depth was completely under the reducing condition with loamy soils in gray color.

For soil pit TA, the reducing conditions indicated by a positive pink color were observed below 55 cm. TA shows a mixed O and A horizon within 30 cm that has a brownish-gray color and very few roots, which is common under hummocks in Western Siberia. Within the 0–55 cm depth, the lateral ring-shaped layers and mud spots can be observed, which were caused by frost heave when a rounded knoll of ice rises during the freezing time. The evidence of cryoturbation can be seen below 55 cm with the dark gray color, and some moss residues are observed in the fragments of cryoturbation clusters.

The vertical elemental concentrations in three soil cores measured by EDX are listed in **Table S1 (Supporting information)** and plotted as logarithmic concentrations in soil core depth in **Figure 2**. The other elements not shown in **Figure 2** did not exhibit a regular pattern under reducing conditions within the soil cores. Mn and Co were enriched in the top mineral layer with organic matter accumulation, which likely because of their complexation with natural organic matter. In contrast, Cr, V, Sr, Ca, Mg, Al, Ti, Cd, Mo, Zr, and Sc increased in lower mineral soil horizons in the three soil cores. In particular, for the MU site, Fe, Cr, and V were only higher in the first gleyed horizon with cryoturbation (7–25 cm) and decreased gradually with increased depth. Al, Ti, Cd, and Sc kept increasing until 40 cm (second gleyed horizon) and then decreased gradually or maintained relatively comparable levels in the deeper layers. As, Mo, and Zr decreased until 40 cm and then increased in deeper mineral horizons mixed with frozen material and at the frozen horizon. Zn, Sr, K, Ca, Na, Mg, and Y

were higher in all gleyed horizons.

For the SY site, three trends were observed: *i*) relatively slight decrease from top to down within the gleyed horizons for As, Cr, V, Mo, Zr, and Se; *ii*) continuous increase in gleyed horizon depth for Sr, K, Ca, Va, Mg, Al, Ti, and Pb; *iii*) only the Cd content increased sharply in the upper gleyed horizon (9–18 cm) and decreased significantly below 18 cm. For the TA site, the maximum concentration was observed in the gleyed horizon for Cr, V, Sr, Ca, Mg, Al, Ti, Cd, Pb, Mo, Zr, Y, and Sc. These elements were apparently enhanced in reducing fractions, concentrations of which, with respect to the upper layers of soil column, can reflect the soils with increased reducing soil conditions. This obvious demarcation between elements with concentrations either increasing in the upper layers of soil column or accumulating in the lower part of soil column correlates to the variation of redox conditions in the soil pit profile as well. The fluctuation of elemental concentrations in the lower soil cores may also be caused by the effect of cryoturbation.

The elemental concentrations of soil porewater are listed in **Table S2** and plotted as the function of depth along the cores (not containing supra-permafrost water) in **Figure 3**. The results showed Ca, Mg, and Ti as soluble species that may be available for transporting supra-permafrost water for all three sites because of the increased concentrations in the deeper fraction of the soil core. Additionally, Al in TA site, Mg in MU site, and Fe in SY site may also have the same potential. To some extent, Mn, Ca, Mg, Al, Ti, and Fe all can be soluble species in both upper and deeper fractions of the soil core, indicating both the transport capability from surface flows and supra-permafrost waters to the river.

3.2 Thermal dynamics within soil depth

The temperatures in multiple depths from the installed thermometers are provided in **Figure 4**. In general, the surface (0 cm) soil temperature corresponds to the variation in ambient temperature in this region. The soils at four different depths in TA, MU, and SY were completely frozen by the end of April as our measurements were initiated. In TA, the thawing of frozen soils (temperature rose above 0 °C) occurred on May 30, 2016 at 0 cm, on June 7,

2016 at 20 cm, on June 18, 2016 at 40 cm, and on June 30, 2016 at 75 cm. In MU, the thawing occurred on June 2, 2016 at 0 cm, on July 14, 2017 at 25 cm, on June 25, 2016 at 40 cm, and on July 4, 2016 on 59 cm. In Sy, the thawing occurred on June 1, 2016 at 0 cm, on June 11, 2016 at 18 cm, on June 22, 2017 at 26 cm, and on July 2, 2016 at 38 cm. The frozen soils in the Arctic notably thaw from top down during the spring-summer season. The lower latitude of TA results in a relatively earlier thawing time than that of MU and SY.

3.3 Chemical composition in the supra-permafrost water

All measured elemental concentrations are plotted as the function of sampling time in **Figure 5** and the pH values for supra-permafrost water in TA, SY, and MU for different sampling months are presented in **Figure S1** with a detailed description in **Text S1**. In TA, the contents of Zn, Mn, Ti, and Sr increased generally from the beginning of summer (June) while Sr and Ti increased slightly with an obvious increasing trend at the end of summer (September 15, 2016). Zn reached its highest concentrations ($15.93\text{--}17.50\ \mu\text{g L}^{-1}$) at the beginning of autumn, and this level was maintained until October 2016. Unlike Zn, the peak value of Mn was observed in October. Fe concentrations started to rise significantly at the end of September and peaked at the end of October 2016 ($2049.71\ \mu\text{g L}^{-1}$). Mg, Cr, V, Pb, Al, and Ca concentrations exhibited less fluctuation over summer with low concentrations until an increasing trend was observed at the beginning of autumn. Na was the only element that showed a gradual increase in concentration over time till October 15, 2016. For Cd and Mo, there was no particular trend, and their levels were low. SY and MU essentially followed the pattern of TA, while the highest Fe concentration in SY was found at the end of October 2016.

3.4 Chemical composition in the surrounding hydrological streams and rivers

We measured the elemental concentrations of the surface water surrounding the soil cores, including the connected hydrological flows (i.e., shallow, depression, and thaw ponds) and rivers (the sites receive the flow), which are shown in **Figure 6**. The pH values for TA, MU,

and SY for different months are shown in **Figure S2** with detailed description in **Text S2**. The concentrations of CO₂, CH₄, and DOC in the surrounding streams are plotted as the function of sampling time in **Figure S3** and described in **Text S3**.

The remaining detected elements were not shown here because they were below the detection limits. The three sites showed strong similarity of elements' distribution in the connected surface flows and the adjacent rivers with the passage of time. Most elements (i.e., Fe, Mn, Zn, Na, Pb, Al, and Ca) showed a dramatically increasing trend from the beginning of September to the beginning of October, while Co, V, and Sr significantly increased beginning in August, and only Cr increased starting in July. These elements in the surrounding hydrological streams or rivers reached their highest concentrations at the beginning of October, except for Mo, Cd, and Ti, which had very low concentrations at all time-scales with a slightly increased concentration in October. The concentrations of Fe, Zn, Al, Co, and Sr were consistent with the observation of enhanced soluble concentrations in supra-permafrost water for each of the corresponding months. This may be because of the solubility of these metals, except Co and Mn, which remained at low levels in the top layers of soil cores, and because of the different solubilities of the metals during snow melting, which are related to the bonding mechanism in the soil, especially for top soil layers with increased organic matter. The highest to lowest concentrations for metals were approximately Fe > Mn > Zn > Sr > Ti > V ≈ Na ≈ Al ≈ Pb > Cd ≈ Mo.

4. Discussion

4.1 Variability of elemental concentrations in solid soil and soil porewater

In the TA soil column, higher elemental concentrations in soil porewater, such as Mn, Mg, and Ti, were found in the oxidizing zone (~10-15 cm, the layer with organic matter accumulations). Compared with the deeper depth of soil column (~30-83 cm, reducing zone), enhanced elemental accumulations were also observed, especially for Mg and Ti. The lesser

extent of Ca and Al concentrations in the top organic layer (**Figure 2**), which may be due to the excess of Ca in the soil solutions, occupy more than 90% of total cation concentration (Leckie 1986). Ca cation can control the soluble stage of trace elements in soils, due to Ca's presentation as an organic complex in soil solutions, preventing the precipitation of soil deposits (Leckie 1986). For instance, fulvic acid in this organic layer can significantly interfere with the crystallization of aluminum hydroxide polymorphs (Kodama and Schnitzer 1980). Besides, the aqueous Ti concentrations in both the oxidizing and reducing zones are similar, while Mn is relatively higher in oxidizing zones, and Mg is more enhanced in the reducing zone. Compared with the distribution of these elements in the solid soil core, only Ca and Al showed a similar trend. This difference is due to the soluble and chemical fraction of species.

In MU soil column, the concentrations of Mn, Ca, Mg, Al, Fe, and Ti in soil porewater were increased below 7 cm in the reduced zones. However, the solid soil phase shows high levels of Mn in the oxidizing zones (~0-7 cm), with the other elements' distribution corresponding to the soluble forms. In SY soil column, Mn, Mg, and Fe contents in soil porewater were enhanced in the upper oxidizing zones, and Ca content was only obviously enhanced in reduced zones, while Al and Ti both accumulated in the oxidizing and reduced zones. The Mn concentrations were found to be the highest in the oxidizing zones in solid phase, whereas other elements (Ca, Mg, Al, Ti, and Fe) increased in the reduced zones.

In both MU and SY, Mn concentrations are found higher in top layer of soil, which is consistent with the low solubility of Mn in lower pH soils (pH = 4.7 for Mu and 4.8 for Sy) (Scholz and Kahlert 2015). We speculate this is because of a more integral gleyed layer (~ 10-40 cm) caused by cryoturbation, which makes the soils share the same origin. SY revealed more heterogenous materials that divided several soil layers through cryoturbation, which results in elemental fluctuations in terms of soluble elements.

The three soil cores' depth represents the typical maximum vertical extent during the thawing period in autumn. Among the three soil cores, differences between elemental

concentrations in soil porewater and solid soil are still substantial. Taking as an example the concentrations of Mn in the Ta soil column, the concentration of Mn in the oxidizing layer is 1039 mg/kg⁻¹ with approximately 0.11 mg/L⁻¹ in soluble form. There is approximately 0.045 mg/L⁻¹ mobilized within thawing water to the reduced zones with 388 mg kg⁻¹ presented in solid soil of this layer.

To better understand the solubility of elements, the partitioning coefficients (K_d) were calculated as shown in **Figure 7**. Despite the discrepancy of K_d below the top layer, the decreasing solubility can be observed within the gleyed layers, which is consistent with the theory that metals are hindered in this layer (Antcibor et al. 2014). However, Al and Mn were observed with clearly increasing solubility in all soil cores above the permafrost table. Besides, the high partitioning from the solid to the aqueous fraction was observed in Ti for Sy, and Fe and Mn for Mu. Unlike the top organic-rich layers mainly reflecting biogeochemical cycle, minerogenic layers reflect mineralogical weathering. Therefore, the difference may be due to different soil textures and frost processes.

The enrichment of Mn and Al for soil materials in Western Siberia was previously investigated (Abakumov et al. 2017, Antcibor et al. 2014, Evgeny et al. 2017, Ji et al. 2019a, Ji et al. 2019b). The further soil water flows into supra-permafrost water, the more it creates consistent input of elements such as Mn and Al from soil to solution. The previous study showed that the solubility of Mn increases with increasing soil acidity (Andrade et al. 2002), which is consistent with our observation. Barker et al. (2014) first reported that trace metals concentrations (Al, Ba, Fe, and Mn) correlate with the seasonal thawed active layer in the Alaskan arctic. This also proves that elemental transport occurred through thawing soil porewater with the potential for those elements to enter surrounding water bodies.

4.2 Elemental fluctuation in supra-permafrost water and surface water by seasonal controls

To some extent, except for Mn and Al, some other elements also showed high solubility in

the bottom of the three soil cores (**Figure 7**). We expected to see high mobilization of Mn, Al, Ca, and Ti to the supra-permafrost water during spring snow thawing. However, except for Mn, no or very slightly increasing concentrations in the late May / beginning of June can be found in the supra-permafrost water (**Figure 5**), which may be due to the low volume of thawing water or the equilibrium between elemental pool size in solid soils and snowmelt water in the reducing zones at this time. We found the peak concentration time for most elements were shown in late autumn / the beginning of winter. Compared with elements in soil porewater, more elements were above the detection limits and at distinguishable higher levels during the August to October time period. This may indicate that the origin of elements in supra-permafrost water may not only originate from the dilution of snowmelt water within the soil core, while other water flows through the slope of the permafrost table in the landscape. The relatively higher levels of elements such as Mn, Zn, and Fe in TA, than that of SY and MU, could result from the frost heaving of the polygon rim, which released more frozen materials. During summer, thawing starts in the permafrost-affected soils leading to a deeper active layer, which can be shown by the slight increase in Mn, Fe and other elemental concentrations in the supra-permafrost water over the course of June, July, and August. This increase is correlated with the low coefficients in the bottom of the soil core, and with the soil temperature as well. The soil thermal stratification shows that soil temperatures were above 0 °C at 0, 20, and 40 cm for TA from late June; in 0, 25, and 40 cm for MU from beginning June; and in 0, 18, and 25 cm for SY from late June whereas the deeper depth (75 cm for TA, 59 for MU, and 38 for SY) was still frozen at this time.

Most elements revealed relatively high solubility with small K_d values at the deepest depth. In Ta, Mn follows this trend at the depth 18-35 cm, whereas at the deeper depth of 35-40 cm the solubility decreases. The high mobility of these elements in the deeper soil column, along with the latter thawing for these layers, could account for high concentrations in supra-permafrost water and surface water in late September and beginning of October. This pattern is relatively comparable to other elements in TA, MU, and SY, except for Ca and Ti in MU.

Generally, elemental fluctuations in the surface flow and river were the same as the supra-permafrost water. The concentrations of Zn, Mn, and Ti in the rivers from July to October were higher than the surface flow, indicating the mobility of these elements to the rivers from the surface flow and include the possibility of contribution to this input from supra-permafrost water. The previous study also showed some metals like Fe, Al, Mn, and Ba decreased in the active layer with subsequent thawing and increasing surface water concentrations during summer to autumn and could indicate elemental transport signals corresponding to the depth dynamics of the active layer (Barker et al. 2014). Our results are consistent with the theory that major and trace elements export to the lakes and rivers through the boundary between the thawed and frozen layers (Raudina et al. 2018). However, we cannot exclude the possibility of abrupt permafrost collapse in the surrounding water body and rivers, which has been shown to enhance metals release into surface water (Loiko et al. 2017). This may also be a reason that not all elements in the surface water were above the detection limits in the soil porewater.

4.3 Potential elemental signatures as a function of organic matter in the surface flow

The discharge and source of water are important for the transport of geochemical components such as elements and organic carbon to surface waters. However, it is difficult to determine water sources in cryogenic landscapes with large amounts of ice and multiple flows. In the present study, DOC is used as the “participating media” to estimate elements transported to the surface water; these are considered to be the major carriers of trace elements in boreal and permafrost-affected organic-rich surface waters (Lyvén et al. 2003, Ma et al. 2019, Neubauer et al. 2013, Rember and Trefry 2004, Vasyukova et al. 2010). Due to no pollution from domestic and industrial activities in our sampling sites, the riverine organic carbon is usually subdivided into two origins as the allochthonous pool derived from terrestrial organic matter (topographical erosion and soil leaching) and the autochthonous

pool derived from in-situ phytoplankton production (Hope et al. 1994). Additionally, an empirical model for organic carbon exports showed DOC exports to surface runoff is mostly driven by the unfrozen zones during permafrost thawing (Fabre et al. 2019). Therefore, the surface streams with smaller water volume connected between the soils and the rivers were investigated for the relationships between DOC and elements, and the elemental relationship among the streams, rivers, and supra-permafrost waters.

The soil in the three study fields all have a top organic layer with sporadic organic distributions in the mineral layers. Previous studies reported that precipitations would form in the rapid surface runoff through supper soil layers with a depth of approximately 15–20 cm (Bishop et al. 1993, Hope et al. 1994). DOC would be exported to the surface water from the top layer without infiltration in the riparian zone. In TA, the highest concentrations of CO₂ and CH₄ were observed in the summer snowmelt season with an increasing thawing degree while low concentrations were observed (**Figure 8**), which may have been due to an abrupt thawing process from the top organic layer. This was consistent with the maximal microbial metabolism occurring at the boundary between thawed and frozen permafrost soils in the Western Siberia lowland (Morgalev et al. 2017). However, Dillon and Molot (1997) reported that the release of CO₂ into the boreal waters was increased when the DOC concentration was elevated in the thermokarst lakes. We found a slight decrease in CO₂ and CH₄ when the DOC concentrations reached its peak in Autumn in TA. However, a different pattern was observed in SY and MU in that CO₂ and CH₄ did not increase significantly during snow-ice melting in the spring and summer seasons, while an increasing trend was observed for DOC contents in the surface water. Manasypov et al. (2015) reported no significant enrichment of CO₂ and CH₄ in the thermokarst water bodies during the spring flood through the base flow and further observed that CO₂ levels only increased in small depressions (<10 m²), which is consistent with the ponds (approximately 1 m²) that we sampled. Although some obvious buildup of CO₂ was found in the summer for SY, the results are still comparable to the phenomena in high latitude lakes (Karlsson et al. 2013). The reason for the contrast between TA and the

other sites (SY and MU) could be caused by the low volume of the water pond in SY, and in MU due to the low ice contents and a short period suitable for this type of accumulation in low elevations. However, there is also a possibility that more ice existing in polygon rim and buried talik would lead more the more unfrozen water flowing to the surrounding streams. Combination of the results of three sites shows that the response mechanism of enhancing CO₂ in the streams during snow melting is heterotrophic respiration of allochthonous DOM, as approved by the constantly elevated DOC concentrations in this period. However, we suggest the bio-utilization of these carbon types in small ponds may vary according to the contents of materials by different water volumes.

The elements with high mobility in the bottom gleyed layer of the soil column and obvious higher concentrations during the snowmelt period were plotted against the DOC (**Figure 8**). In Ta, Mn increased sharply in the summer while Al, Ca, and Mg did not significantly increase. Peak values of Mn, Al, Ca, and Mg with DOC were observed in autumn. The same pattern was observed for SY and MU, especially for Mn. This may indicate the release of micronutrients as Mn during vegetation activity and upper moss litter leaching in the warmer water, which allows higher mobility within the soil column. Because we did not observe a high concentration of Mn in the uppermost soil layer (**Figure 2**), we speculate this contribution of Mn may be from the supra-permafrost water.

Another difference found in the TA site was that elemental concentrations (Al, Ca, and Mg) in autumn were significantly higher in comparison to MU and SY, which may be a result of upwelling via the icy cracks beginning as early as October, producing organic- and Fe-accumulated allochthonous ice crystallized at the pond surface. The maximum values of these elements peak during autumn in the surface water are about 2 to 3 times greater than in spring and summer, representing the highest water flow including DOC and dissolved elements.

Additionally, the strong linear correlation of Mn between surface streams and rivers was found for all three sites, and that of Al between the surface streams and river was found for Ta (**Figure 9**). However, when comparing the surface streams and supra-permafrost water, Mn

was correlated for all three sites; Al only for TA and SY; and Ca only for TA (**Figure 10**). For Mn, the snowmelt flows had higher Mn contents attributed to the increasing mobility of Mn species to other elements in superficial layers of soil as previously reported (Barker et al. 2014). Supra-permafrost water also initially contributes to the surface flows and then further flows to the river. The differences for Al and Ca may be due to the different water–soil interactions. Therefore, Mn could be a seasonal signature of autumn representing the dominance of overland surface flow and maximum interactions with the active layer when the active layer is the deepest.

5. Conclusion

This study found that the levels of elements did not begin to increase when the surface temperature is above 0 °C, and the deeper soil column temperature is above 0 °C in late summer/early autumn. The patterns for surrounding water ponds, adjacent river surface waters, and supra-permafrost waters were generally comparable for most elements above detection limits (Zn, Mn, Sr, Fe, Mg, Cr, Co, V, Pb, Al, and Ca) and were highest during the period from September to October, corresponding to the deepest depth of the active layer. Although a geochemical barrier in the reducing gleyed layers was observed in the soil column, some elements (Mn, Ca, Mg, Al, and Ti) still have high mobility above the permafrost table. Additionally, Mn may flow into surrounding water flows (to the river) by both upper soil and supra-permafrost waters transporting organic matter including CH₄ and CO₂. However, heterogenous landscapes with more ice and cryoturbation may cause more elements to move to the surface waters in the present study. Mn in surface flow may be a proxy for the active layer process during the period of summer and autumn. Highly dynamic Arctic hydrological systems that receive geochemical elements from surrounding permafrost soils and delivering more DOC and elements to adjacent hydrological systems. Future climate conditions will intensify the soil–stream–river process due to permafrost degradation and the dynamics of the active layer.

601 **Acknowledgements**

602 This work was supported by a grant from the Russian Foundation for Basic research (18-
603 44-890003, 16-34-60010 and 19-416-890002); by Jiangsu Nature Science Fund
604 (BK20151378) and the Fundamental Research Funds for the Central Universities
605 (090514380001); by a grant from Saint-Petersburg State University "Urbanized ecosystems of
606 the Russian Arctic: dynamics; state and sustainable development (grant number: 39377455)".
607 We would like to thank Miss Yu Su from the School of Visual Arts at BFA Computer Art for
608 helping with data visualization, and Miss Kuznetsova Ekaterina from School of Journalism
609 and Communication, Tsinghua University for helping with the Russian translation. All data
610 used in figures for analysis are provided in uploaded file "raw data".

611 References

- 612 Abakumov, E., Shamilishvili, G. and Yurtaev, A. (2017) Soil polychemical contamination on
 613 Belyi Island as key background and reference plot for Yamal region, p. 313.
- 614 Alekseev, I. and Abakumov, E. (2018) Permafrost-affected former agricultural soils of the
 615 Salekhard city (Central part of Yamal region).
- 616 Andrade, E., Miyazawa, M., Pavan, M.A. and Oliveira, E.L.d. (2002) Effect of Organic
 617 Matter on Manganese Solubility. *Brazilian Archives of Biology and Technology* 45, 17-20.
- 618 Antcibor, I., Eschenbach, A., Zubrzycki, S., Kutzbach, L., Bolshiyarov, D. and Pfeiffer, E.M.
 619 (2014) Trace metal distribution in pristine permafrost-affected soils of the Lena River delta
 620 and its hinterland, northern Siberia, Russia. *Biogeosciences* 11(1), 1-15.
- 621 Barker, A.J., Douglas, T.A., Jacobson, A.D., McClelland, J.W., Ilgen, A.G., Khosh, M.S.,
 622 Lehn, G.O. and Trainor, T.P. (2014) Late season mobilization of trace metals in two small
 623 Alaskan arctic watersheds as a proxy for landscape scale permafrost active layer dynamics.
 624 *Chemical Geology* 381, 180-193.
- 625 Bespalaya, Y., Aksenova, O. and Zubriy, N. (2018) Molluscan fauna of the lower reaches of
 626 the Syoyakha River (Yamal Peninsula). *Arctic Environmental Research* 18, 76-81.
- 627 Bishop, K.H., Lundström, U.S. and Giesler, R. (1993) Transfer of organic C from forest soils
 628 to surface waters: example from northern Sweden. *Applied Geochemistry* 8, 11-15.
- 629 Brown, N.J., Nilsson, J. and Pemberton, P. (2019) Arctic Ocean Freshwater Dynamics:
 630 Transient Response to Increasing River Runoff and Precipitation. *Journal of Geophysical*
 631 *Research-Oceans* 124(7), 5205-5219.
- 632 Cederstrom, D.J., Johnston, P.M. and Subitzky, S. (1953) Occurrence and development of
 633 ground water in permafrost regions.
- 634 Christiansen, H.H., Etzelmüller, B., Isaksen, K., Juliussen, H., Farbrøt, H., Humlum, O.,
 635 Johansson, M., Ingeman-Nielsen, T., Kristensen, L., Hjort, J., Holmlund, P., Sannel, A.B.K.,
 636 Sigsgaard, C., Åkerman, H.J., Foged, N., Blikra, L.H., Pernosky, M.A. and Ødegård, R.S.
 637 (2010) The thermal state of permafrost in the nordic area during the international polar year
 638 2007–2009. *Permafrost and Periglacial Processes* 21(2), 156-181.
- 639 Colombo, N., Salerno, F., Martin, M., Malandrino, M., Giardino, M., Serra, E., Godone, D.,
 640 Said-Pullicino, D., Fratianni, S., Paro, L., Tartari, G. and Freppaz, M. (2019) Influence of
 641 permafrost, rock and ice glaciers on chemistry of high-elevation ponds (NW Italian Alps).
 642 *Science of the Total Environment* 685, 886-901.
- 643 Connon, R., Devoie, E., Hayashi, M., Veness, T. and Quinton, W. (2018) The Influence of
 644 Shallow Taliks on Permafrost Thaw and Active Layer Dynamics in Subarctic Canada. *Journal*
 645 *of Geophysical Research-Earth Surface* 123(2), 281-297.
- 646 Dillon, P.J. and Molot, L.A. (1997) Dissolved organic and inorganic carbon mass balances in
 647 central Ontario lakes. *Biogeochemistry* 36(1), 29-42.
- 648 Dvornikov, Y.A., Leibman, M.O., Khomutov, A.V., Kizyakov, A.I., Semenov, P., Bussmann,
 649 I., Babkin, E.M., Heim, B., Portnov, A., Babkina, E.A., Streletskaya, I.D., Chetverova, A.A.,
 650 Kozachek, A. and Meyer, H. (2019) Gas-emission craters of the Yamal and Gydan peninsulas:

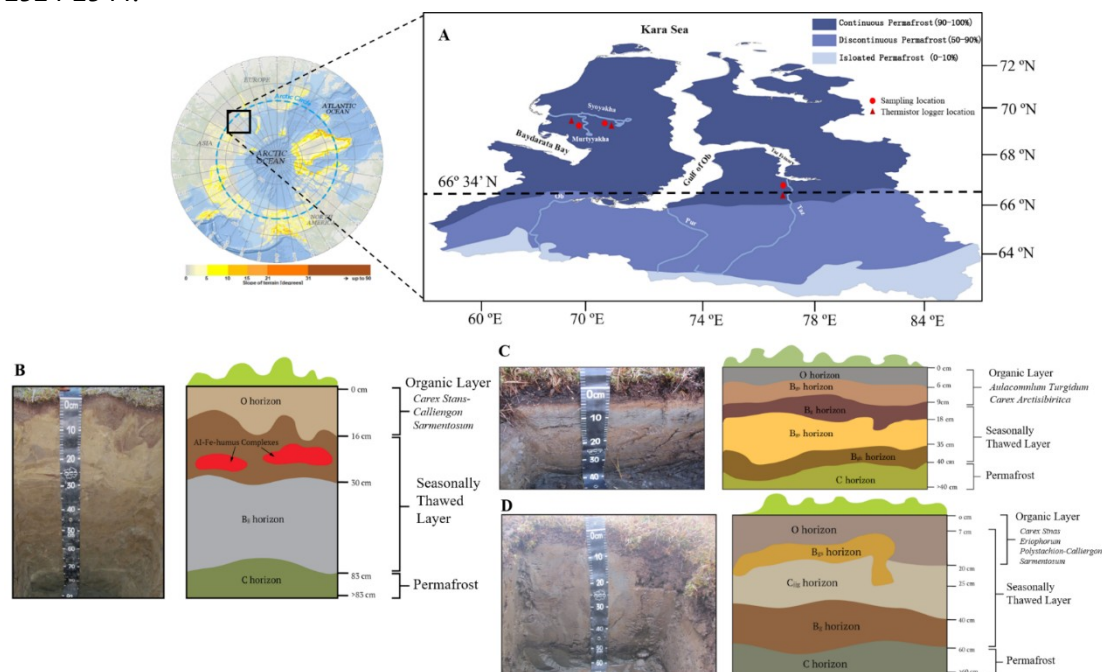
- 651 A proposed mechanism for lake genesis and development of permafrost landscapes.
 652 Permafrost and Periglacial Processes 30(3), 146-162.
- 653 Elder, C.D., Schweiger, M., Lam, B., Crook, E.D., Xu, X., Walker, J., Anthony, K.M.W. and
 654 Czimczik, C.I. (2019) Seasonal Sources of Whole-Lake CH₄ and CO₂ Emissions From
 655 Interior Alaskan Thermokarst Lakes. Journal of Geophysical Research-Biogeosciences
 656 124(5), 1209-1229.
- 657 Evgeny, L., Beznosikov, V. and Abakumov, E. (2017) Humic substances elemental
 658 composition of selected taiga and tundra soils from Russian European North-East. Polish
 659 Polar Research 38, 125-147.
- 660 Fabre, C., Sauvage, S., Tananaev, N., Noël, G.E., Teisserenc, R., Probst, J.L. and Pérez, J.M.S.
 661 (2019) Assessment of sediment and organic carbon exports into the Arctic ocean: The case of
 662 the Yenisei River basin. Water Research 158, 118-135.
- 663 Feng, D., Gleason, C.J., Yang, X. and Pavelsky, T.M. (2019) Comparing Discharge Estimates
 664 Made via the BAM Algorithm in High-Order Arctic Rivers Derived Solely From Optical
 665 CubeSat, Landsat, and Sentinel-2 Data. Water Resources Research.
- 666 Golovatin, M., Morozova, L.M., Ektova, S.N. and Paskhalny, S.P. (2011) The change of
 667 tundra biota at Yamal Peninsula (the north of the Western Siberia, Russia) in connection with
 668 anthropogenic and climatic shifts. Tundras: Vegetation, Wildlife and Climate Trends, 1-46.
- 669 Grosse, G., Goetz, S., McGuire, A.D., Romanovsky, V.E. and Schuur, E.A.G. (2016)
 670 Changing permafrost in a warming world and feedbacks to the Earth system. Environmental
 671 Research Letters 11(4), 040201.
- 672 Guo, L., Ping, C.-L. and Macdonald, R.W. (2007) Mobilization pathways of organic carbon
 673 from permafrost to arctic rivers in a changing climate. Geophysical Research Letters 34(13).
- 674 Hope, D., Billett, M.F. and Cresser, M.S. (1994) A review of the export of carbon in river
 675 water: Fluxes and processes. Environmental Pollution 84(3), 301-324.
- 676 Jessen, S., Holmslykke, H.D., Rasmussen, K., Richardt, N. and Holm, P.E. (2014) Hydrology
 677 and pore water chemistry in a permafrost wetland, Ilulissat, Greenland. Water Resources
 678 Research 50(6), 4760-4774.
- 679 Ji, X., Abakumov, E., Antcibor, I., Tomashunas, V., Knoblauch, C., Zubzycki, S. and Pfeiffer,
 680 E.-M. (2019a) Influence of Anthropogenic Activities on Metals in Arctic Permafrost: A
 681 Characterization of Benchmark Soils on the Yamal and Gydan Peninsulas in Russia. Archives
 682 of Environmental Contamination and Toxicology 76(4), 540-553.
- 683 Ji, X., Abakumov, E. and Polyakov, V. (2019b) Assessments of pollution status and human
 684 health risk of heavy metals in permafrost-affected soils and lichens: A case-study in Yamal
 685 Peninsula, Russia Arctic AU - Ji, Xiaowen. Human and Ecological Risk Assessment: An
 686 International Journal, 1-18.
- 687 Johnson, K.D., Harden, J.W., David McGuire, A., Clark, M., Yuan, F. and Finley, A.O. (2013)
 688 Permafrost and organic layer interactions over a climate gradient in a discontinuous
 689 permafrost zone. Environmental Research Letters 8(3), 035028.
- 690 Johnston, C.E., Ewing, S.A., Harden, J.W., Varner, R.K., Wickland, K.P., Koch, J.C., Fuller,
 691 C.C., Manies, K. and Jorgenson, M.T. (2014) Effect of permafrost thaw on CO₂ and
 692 CH₄ exchange in a western Alaska peatland chronosequence. Environmental Research Letters
 693 9(8), 085004.
- 694 Jorgenson, M.T., Romanovsky, V., Harden, J., Shur, Y., O'Donnell, J., Schuur, E.A.G.,

- Kanevskiy, M. and Marchenko, S. (2010) Resilience and vulnerability of permafrost to climate change. *Canadian Journal of Forest Research* 40(7), 1219-1236.
- Karlsson, J., Giesler, R., Persson, J. and Lundin, E. (2013) High emission of carbon dioxide and methane during ice thaw in high latitude lakes. *Geophysical Research Letters* 40(6), 1123-1127.
- Kastanidis, P., Michalis, V.K., Romanos, G.E., Stubos, A.K., Economou, I.G. and Tsimpanogiannis, I.N. (2018) Solubility of Methane and Carbon Dioxide in the Aqueous Phase of the Ternary (Methane + Carbon Dioxide + Water) Mixture: Experimental Measurements and Molecular Dynamics Simulations. *Journal of Chemical & Engineering Data* 63(4), 1027-1035.
- Keller, K., Blum, J.D. and Kling, G.W. (2007) Geochemistry of Soils and Streams on Surfaces of Varying Ages in Arctic Alaska. *Arctic, Antarctic, and Alpine Research* 39(1), 84-98.
- Keller, K., Blum, J.D. and Kling, G.W. (2010) Stream geochemistry as an indicator of increasing permafrost thaw depth in an arctic watershed. *Chemical Geology* 273(1), 76-81.
- Kodama, H. and Schnitzer, M. (1980) Effect of fulvic acid on the crystallization of aluminum hydroxides. *Geoderma* 24(3), 195-205.
- Lamhonwah, D., Lafrenière, M.J., Lamoureux, S.F. and Wolfe, B.B. (2017) Evaluating the hydrological and hydrochemical responses of a High Arctic catchment during an exceptionally warm summer. *Hydrological Processes* 31(12), 2296-2313.
- Lammers, R.B., Shiklomanov, A.I., Vorosmarty, C.J., Fekete, B.M. and Peterson, B.J. (2001) Assessment of contemporary Arctic river runoff based on observational discharge records. *Journal of Geophysical Research-Atmospheres* 106(D4), 3321-3334.
- Leckie, J.O. (1986) Adsorption and Transformation of Trace Element Species at Sediment/Water Interfaces. Bernhard, M., Brinckman, F.E. and Sadler, P.J. (eds), pp. 237-254, Springer Berlin Heidelberg, Berlin, Heidelberg.
- Liljedahl, A.K., Boike, J., Daanen, R.P., Fedorov, A.N., Frost, G.V., Grosse, G., Hinzman, L.D., Iijima, Y., Jorgenson, J.C., Matveyeva, N., Necsoiu, M., Reynolds, M.K., Romanovsky, V.E., Schulla, J., Tape, K.D., Walker, D.A., Wilson, C.J., Yabuki, H. and Zona, D. (2016) Pan-Arctic ice-wedge degradation in warming permafrost and its influence on tundra hydrology. *Nature Geoscience* 9(4), 312-+.
- Loiko, S.V., Pokrovsky, O.S., Raudina, T.V., Lim, A., Kolesnichenko, L.G., Shirokova, L.S., Vorobyev, S.N. and Kirpotin, S.N. (2017) Abrupt permafrost collapse enhances organic carbon, CO₂, nutrient and metal release into surface waters. *Chemical Geology* 471, 153-165.
- Lyvén, B., Hassellöv, M., Turner, D.R., Haraldsson, C. and Andersson, K. (2003) Competition between iron- and carbon-based colloidal carriers for trace metals in a freshwater assessed using flow field-flow fractionation coupled to ICPMS. *Geochimica et Cosmochimica Acta* 67(20), 3791-3802.
- Ma, Q., Jin, H., Yu, C. and Bense, V.F. (2019) Dissolved organic carbon in permafrost regions: A review. *Science China Earth Sciences* 62(2), 349-364.
- Manasypov, R.M., Vorobyev, S.N., Loiko, S.V., Kritzkov, I.V., Shirokova, L.S., Shevchenko, V.P., Kirpotin, S.N., Kulizhsky, S.P., Kolesnichenko, L.G., Zemtsov, V.A., Sinkinov, V.V. and Pokrovsky, O.S. (2015) Seasonal dynamics of organic carbon and metals in thermokarst lakes from the discontinuous permafrost zone of western Siberia. *Biogeosciences* 12(10), 3009-

- 739 3028.
- 740 McClelland, J.W., Stieglitz, M., Pan, F., Holmes, R.M. and Peterson, B.J. (2007) Recent
741 changes in nitrate and dissolved organic carbon export from the upper Kuparuk River, North
742 Slope, Alaska. *Journal of Geophysical Research: Biogeosciences* 112(G4).
- 743 McCurdy, E. and Woods, G. (2004) The application of collision/reaction cell inductively
744 coupled plasma mass spectrometry to multi-element analysis in variable sample matrices,
745 using He as a non-reactive cell gas. *Journal of Analytical Atomic Spectrometry* 19(5), 607-
746 615.
- 747 Morgalev, Y.N., Lushchaeva, I.V., Morgaleva, T.G., Kolesnichenko, L.G., Loiko, S.V.,
748 Krickov, I.V., Lim, A., Raudina, T.V., Volkova, I.I., Shirokova, L.S., Morgalev, S.Y.,
749 Vorobyev, S.N., Kirpotin, S.N. and Pokrovsky, O.S. (2017) Bacteria primarily metabolize at
750 the active layer/permafrost border in the peat core from a permafrost region in western
751 Siberia. *Polar Biology* 40(8), 1645-1659.
- 752 Natali, S.M., Schuur, E.A.G., Mauritz, M., Schade, J.D., Celis, G., Crummer, K.G., Johnston,
753 C., Krapek, J., Pegoraro, E., Salmon, V.G. and Webb, E.E. (2015) Permafrost thaw and soil
754 moisture driving CO₂ and CH₄ release from upland tundra. *Journal of Geophysical*
755 *Research: Biogeosciences* 120(3), 525-537.
- 756 Neubauer, E., Köhler, S.J., von der Kammer, F., Laudon, H. and Hofmann, T. (2013) Effect of
757 pH and Stream Order on Iron and Arsenic Speciation in Boreal Catchments. *Environmental*
758 *Science & Technology* 47(13), 7120-7128.
- 759 Olefeldt, D. and Roulet, N.T. (2012) Effects of permafrost and hydrology on the composition
760 and transport of dissolved organic carbon in a subarctic peatland complex. *Journal of*
761 *Geophysical Research: Biogeosciences* 117(G1), 页码.
- 762 Ping, C.-L., Clark, M.H., Kimble, J.M., Michaelson, G.J., Shur, Y. and Stiles, C.A. (2013)
763 Sampling Protocols for Permafrost-Affected Soils. *Soil Horizons* 54(1), 页码.
- 764 Ping, C.L., Bockheim, J.G., Kimble, J.M., Michaelson, G.J. and Walker, D.A. (1998)
765 Characteristics of cryogenic soils along a latitudinal transect in Arctic Alaska. *Journal of*
766 *Geophysical Research-Atmospheres* 103(D22), 28917-28928.
- 767 Pokrovsky, O.S., Manasypov, R.M., Loiko, S.V., Krickov, I.A., Kopysov, S.G.,
768 Kolesnichenko, L.G., Vorobyev, S.N. and Kirpotin, S.N. (2016a) Trace element transport in
769 western Siberian rivers across a permafrost gradient. *Biogeosciences* 13(6), 1877-1900.
- 770 Pokrovsky, O.S., Manasypov, R.M., Loiko, S.V. and Shirokova, L.S. (2016b) Organic and
771 organo-mineral colloids in discontinuous permafrost zone. *Geochimica et Cosmochimica Acta*
772 188, 1-20.
- 773 Pokrovsky, O.S., Shirokova, L.S., Kirpotin, S.N., Audry, S., Viers, J. and Dupre, B. (2011)
774 Effect of permafrost thawing on organic carbon and trace element colloidal speciation in the
775 thermokarst lakes of western Siberia. *Biogeosciences* 8(3), 565-583.
- 776 Polishchuk, Y.M., Bogdanov, A.N., Muratov, I.N., Polishchuk, V.Y., Lim, A., Manasypov,
777 R.M., Shirokova, L.S. and Pokrovsky, O.S. (2018) Minor contribution of small thaw ponds to
778 the pools of carbon and methane in the inland waters of the permafrost-affected part of the
779 Western Siberian Lowland. *Environmental Research Letters* 13(4), 页码.
- 780 Raudina, T.V., Loiko, S.V., Lim, A., Manasypov, R.M., Shirokova, L.S., Istigechev, G.I.,
781 Kuzmina, D.M., Kulizhsky, S.P., Vorobyev, S.N. and Pokrovsky, O.S. (2018) Permafrost thaw
782 and climate warming may decrease the CO₂, carbon, and metal concentration in peat soil

- 783 waters of the Western Siberia Lowland. *Science of the Total Environment* 634, 1004-1023.
- 784 Rember, R.D. and Trefry, J.H. (2004) Increased concentrations of dissolved trace metals and
 785 organic carbon during snowmelt in rivers of the alaskan arctic 1 Associate editor: K. F.
 786 Falkner. *Geochimica et Cosmochimica Acta* 68(3), 477-489.
- 787 Romanovsky, V.E., Drozdov, D.S., Oberman, N.G., Malkova, G.V., Kholodov, A.L.,
 788 Marchenko, S.S., Moskalenko, N.G., Sergeev, D.O., Ukraintseva, N.G., Abramov, A.A.,
 789 Gilichinsky, D.A. and Vasiliev, A.A. (2010) Thermal state of permafrost in Russia. *Permafrost
 790 and Periglacial Processes* 21(2), 136-155.
- 791 Scholz, F. and Kahlert, H. (2015) The calculation of the solubility of metal hydroxides, oxide-
 792 hydroxides, and oxides, and their visualisation in logarithmic diagrams. *ChemTexts* 1(1), 7.
- 793 Schuur, E.A.G., McGuire, A.D., Schädel, C., Grosse, G., Harden, J.W., Hayes, D.J., Hugelius,
 794 G., Koven, C.D., Kuhry, P., Lawrence, D.M., Natali, S.M., Olefeldt, D., Romanovsky, V.E.,
 795 Schaefer, K., Turetsky, M.R., Treat, C.C. and Vonk, J.E. (2015) Climate change and the
 796 permafrost carbon feedback. *Nature* 520, 171.
- 797 Sidorchuk, A. and Grigorev, V. (1998) Soil erosion on the Yamal peninsula (Russian Arctic)
 798 due to gas field exploitation , 出版社 , 出版城市.
- 799 Smith, S.L., Romanovsky, V.E., Lewkowicz, A.G., Burn, C.R., Allard, M., Clow, G.D.,
 800 Yoshikawa, K. and Throop, J. (2010) Thermal state of permafrost in North America: a
 801 contribution to the international polar year. *Permafrost and Periglacial Processes* 21(2), 117-
 802 135.
- 803 Street, L.E., Dean, J.F., Billett, M.F., Baxter, R., Dinsmore, K.J., Lessels, J.S., Subke, J.-A.,
 804 Tetzlaff, D. and Wookey, P.A. (2016) Redox dynamics in the active layer of an Arctic
 805 headwater catchment; examining the potential for transfer of dissolved methane from soils to
 806 stream water. *Journal of Geophysical Research: Biogeosciences* 121(11), 2776-2792.
- 807 Tarnocai, C. (2009) Permafrost Soils. Margesin, R. (ed), pp. 3-16, Springer Berlin Heidelberg,
 808 Berlin, Heidelberg.
- 809 Vasil'chuk, Y., Budantseva, N., Vasil'chuk, A., Chizhova, J., Podborny, Y. and Vasil'chuk, J.
 810 (2016) Holocene multistage massive ice, Sabettayakha river mouth, Yamal Peninsula,
 811 northwest Siberia. *GeoResJ* 9-12, 54-66.
- 812 Vasyukova, E.V., Pokrovsky, O.S., Viers, J., Oliva, P., Dupré, B., Martin, F. and Candaudap, F.
 813 (2010) Trace elements in organic- and iron-rich surficial fluids of the boreal zone: Assessing
 814 colloidal forms via dialysis and ultrafiltration. *Geochimica et Cosmochimica Acta* 74(2), 449-
 815 468.
- 816 Walvoord, M.A. and Striegl, R.G. (2007) Increased groundwater to stream discharge from
 817 permafrost thawing in the Yukon River basin: Potential impacts on lateral export of carbon
 818 and nitrogen. *Geophysical Research Letters* 34(12).
- 819 Wild, B., Andersson, A., Broder, L., Vonk, J., Hugelius, G., McClelland, J.W., Song, W.,
 820 Raymond, P.A. and Gustafsson, O. (2019) Rivers across the Siberian Arctic unearth the
 821 patterns of carbon release from thawing permafrost. *Proceedings of the National Academy of
 822 Sciences of the United States of America* 116(21), 10280-10285.
- 823 WRB (2015) World reference base (WRB) for soil resources, International soil classification
 824 system for naming soils and creating legends for soil maps. Food and Agriculture organization
 825 of the united nation (FAO), Rome.
- 826 Yang, D.Q., Kane, D.L., Hinzman, L.D., Zhang, X.B., Zhang, T.J. and Ye, H.C. (2002)

827 Siberian Lena River hydrologic regime and recent change. Journal of Geophysical Research-
 828 Atmospheres 107(D23).
 829 Zheng, L., Overeem, I., Wang, K. and Clow, G.D. (2019) Changing Arctic River Dynamics
 830 Cause Localized Permafrost Thaw. Journal of Geophysical Research-Earth Surface 124(9),
 831 2324-2344.



832 **Figure 1.** Location of the sampling area and installed thermometer (A). Soil pit profiles and their
 833 upper vegetation species near rivers: (B) Taz river (67°30'13.3"N, 78°40'56.2"E), (C) Syoyakha
 834 river (69°57'03.6"N, 71°23'15.2"E), and (D) Murtyyakha river (70°06'04.7"N, 68°40'24.1"E) in
 835 Yamal-Nets Autonomous Region. All soil profiles are gleyed and have oxidation/reduction
 836 horizons in the upper active layer, substantial top organic layer, and cryoturbation in the lower part
 837 of the active layer.
 838
 839

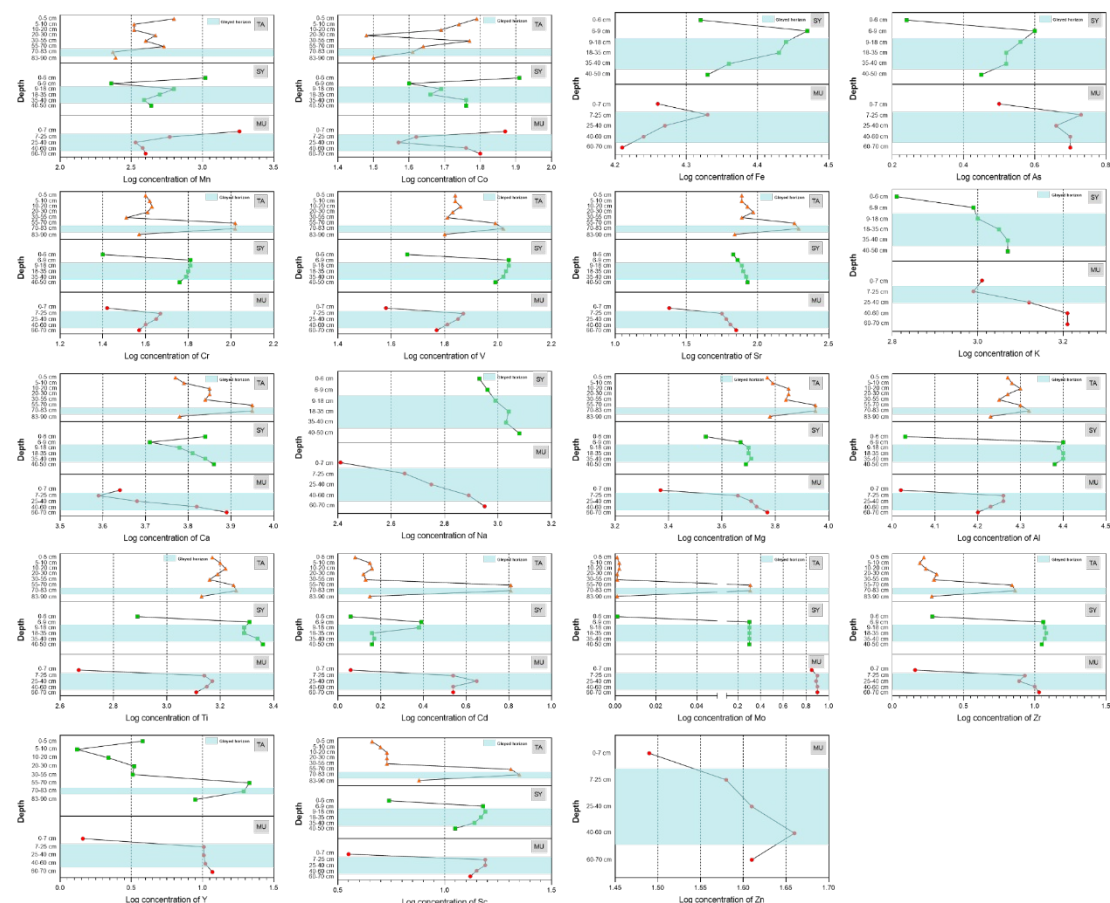
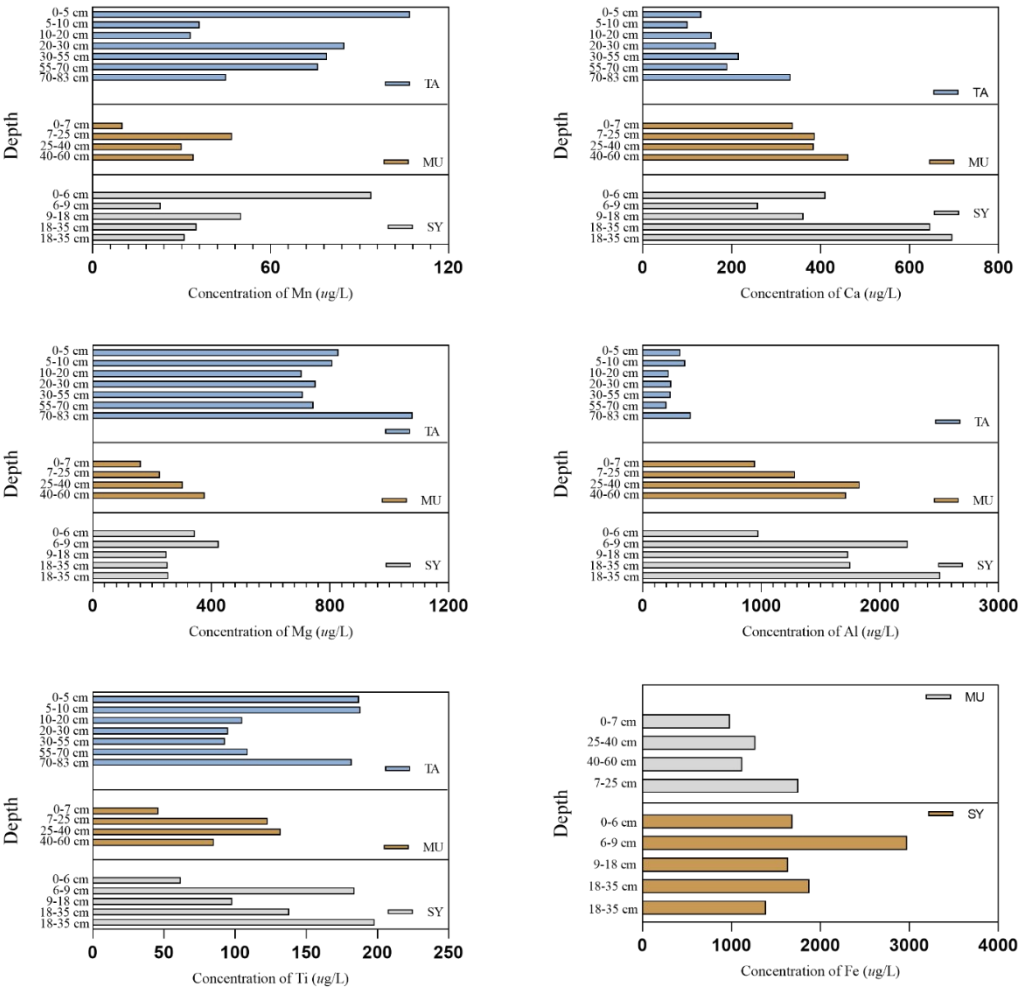
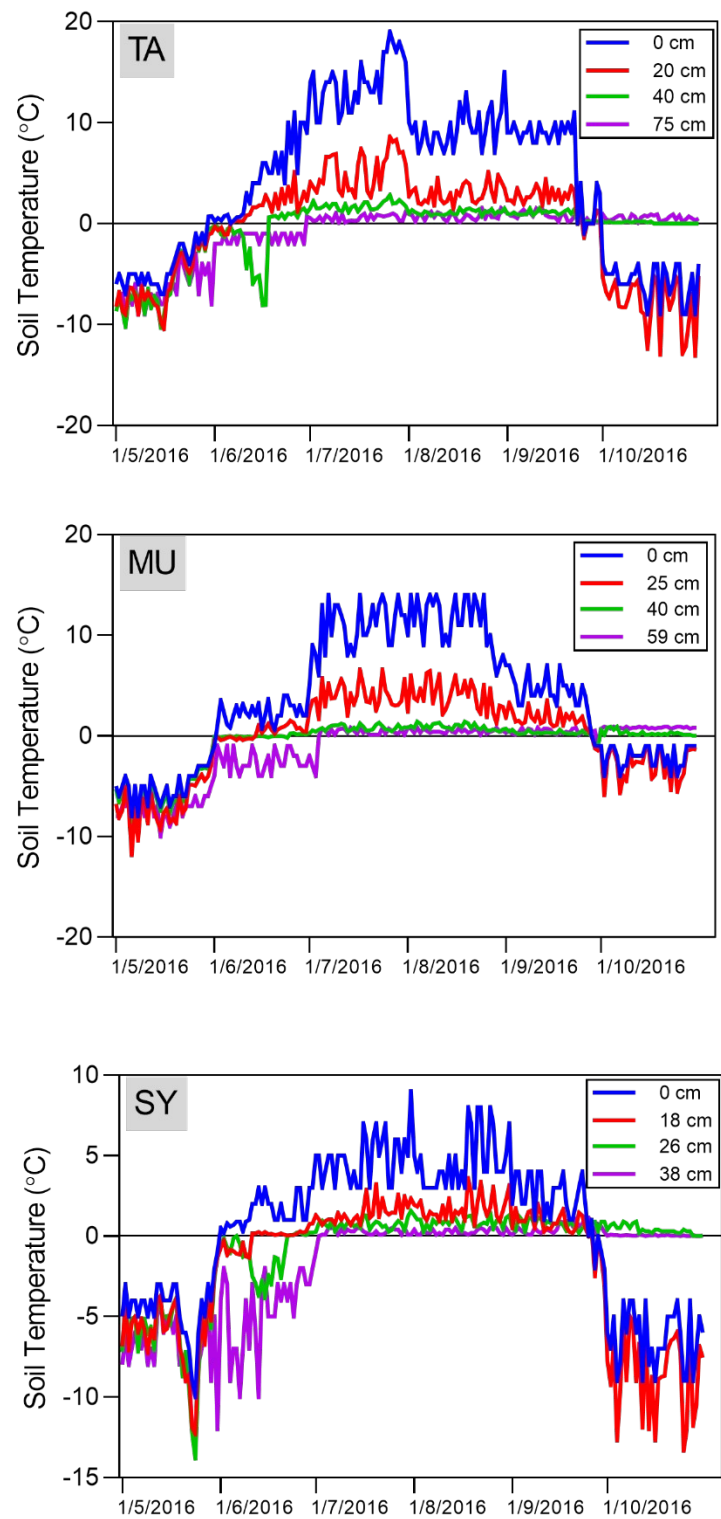


Figure 2. Vertical metal/element distribution in soil cores collected from TA (Taz river), SY (Syoyakha river) and MU (Murtyyakha river) sites in the Yamal-Nets Autonomous Region in beginning May 2016. The logarithmic transformed distribution shows the elements' enrichment relevant to the top layer with humus accumulation in an oxidizing condition (Mn and Co) and the lower gleyed layer in a reducing condition.



848 **Figure 3.** Distributions of soluble metals along the vertical soil water extracted from the soil
849 cores collected adjacent to the Ta, Sy, and Mu rivers in the Yamal-Nets Autonomous Region.



850
851 **Figure 4.** Soil temperature (°C) at different soil depths within the active layer as function of
852 time in 2016. The soil in the Russian Arctic (TA, SY, and MU sites) experiences a top to down
853 freezing process, making soil porewater flow downwards to deeper soils above frozen
854 materials (permafrost table).
855

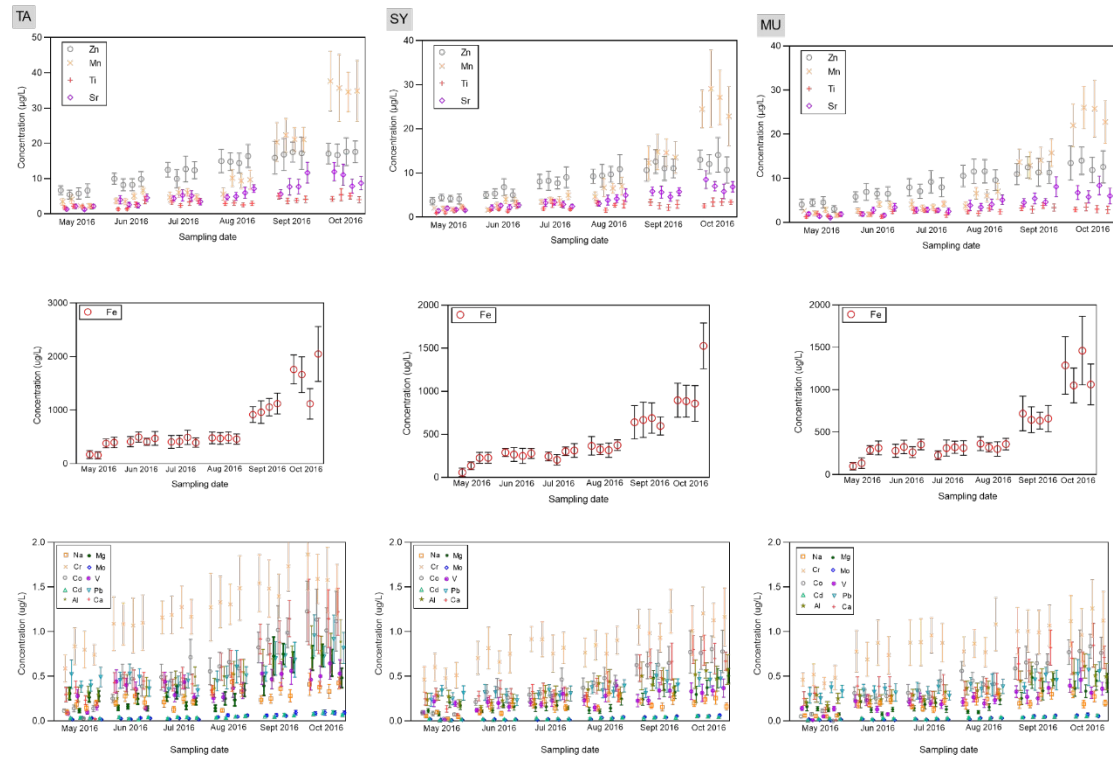


Figure 5. Soluble element concentrations ($\mu\text{g/L}$) in the supra-permafrost water collected from the Ta, Sy and Mu sites as a function of date in 2016, respectively.

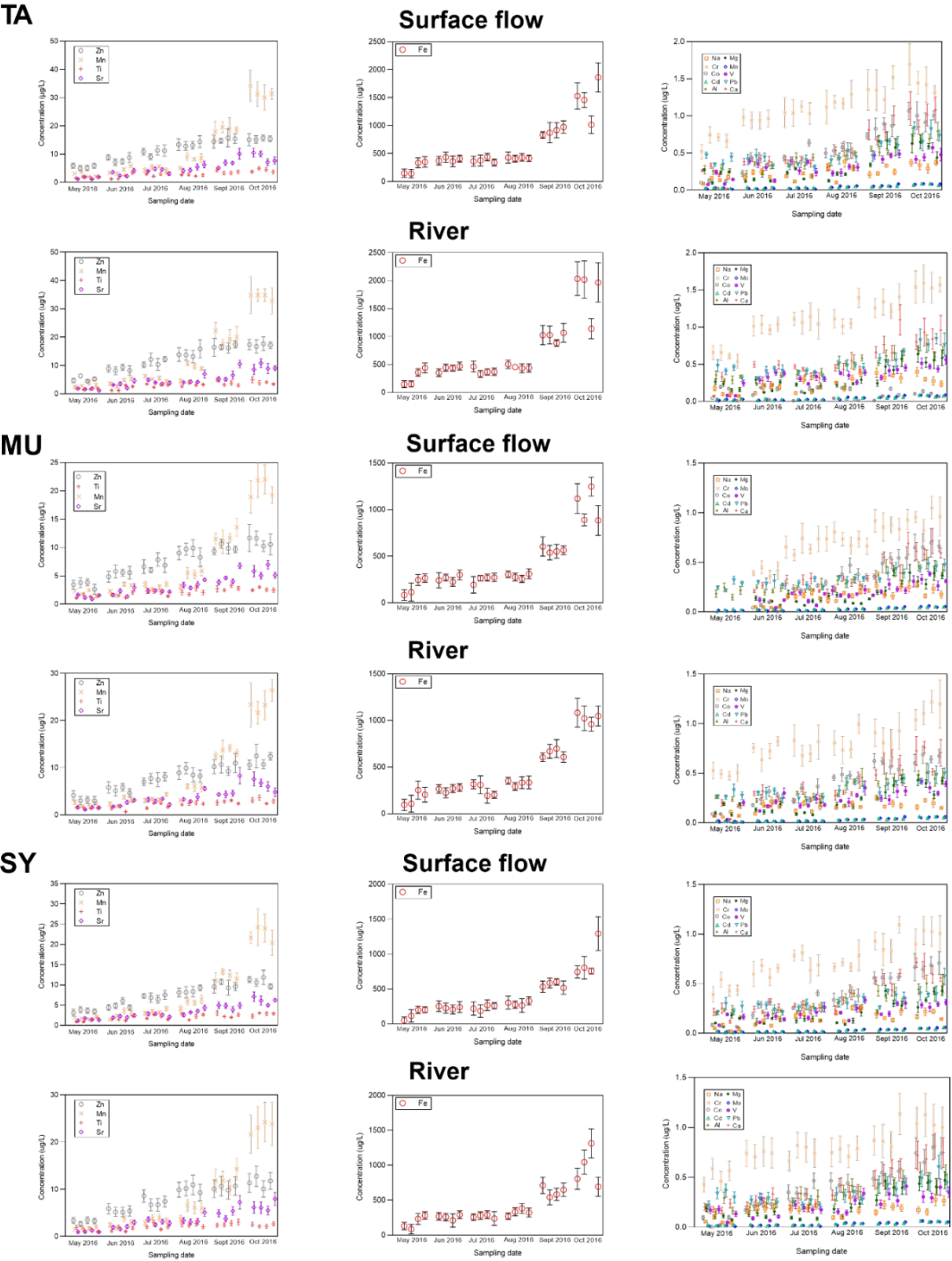
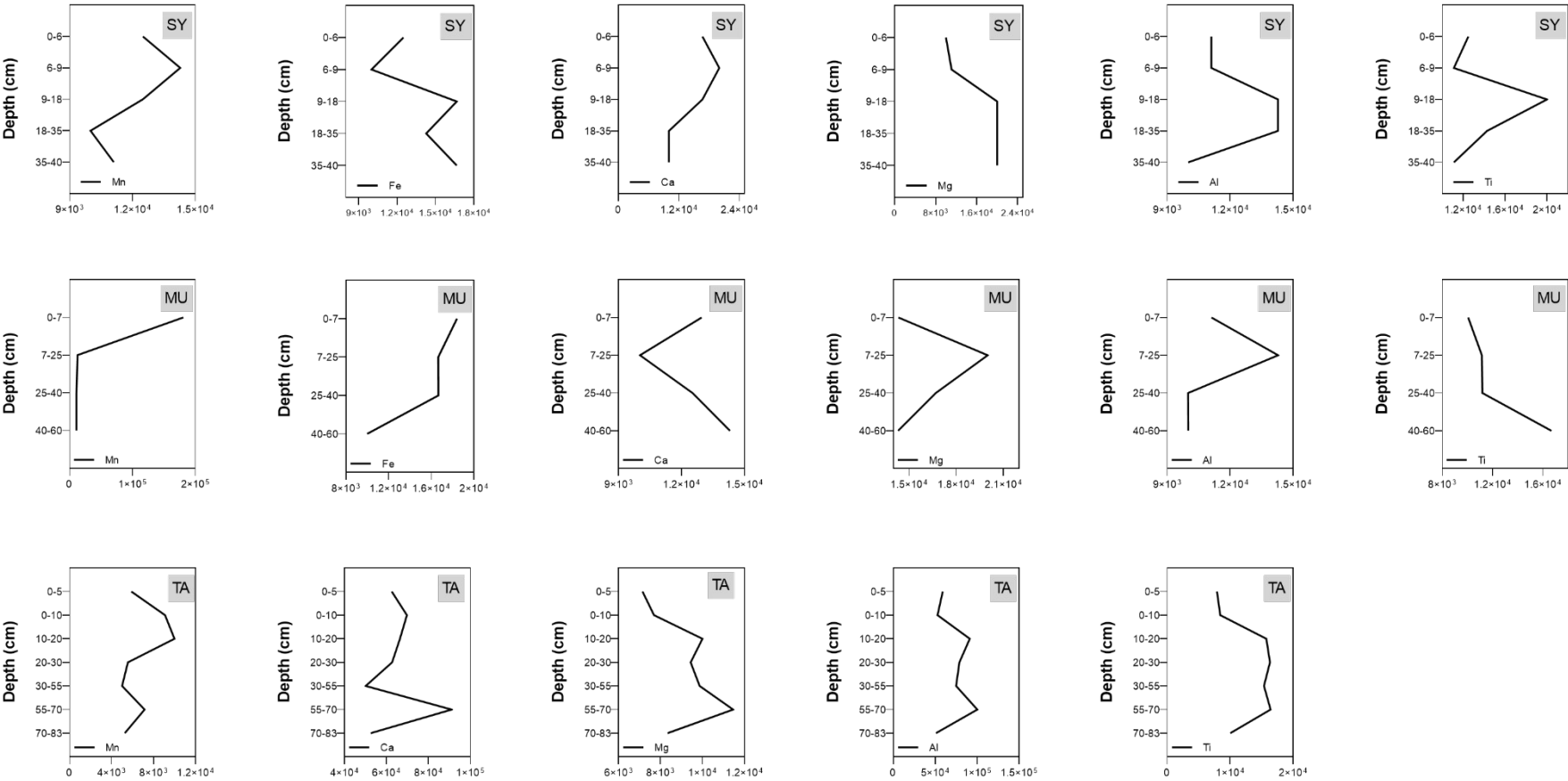


Figure 6. Soluble element concentrations (µg/L) in the surface water from connected hydrological streams to rivers and rivers from the TA, SY, and MU sites as a function of date in 2016, respectively.



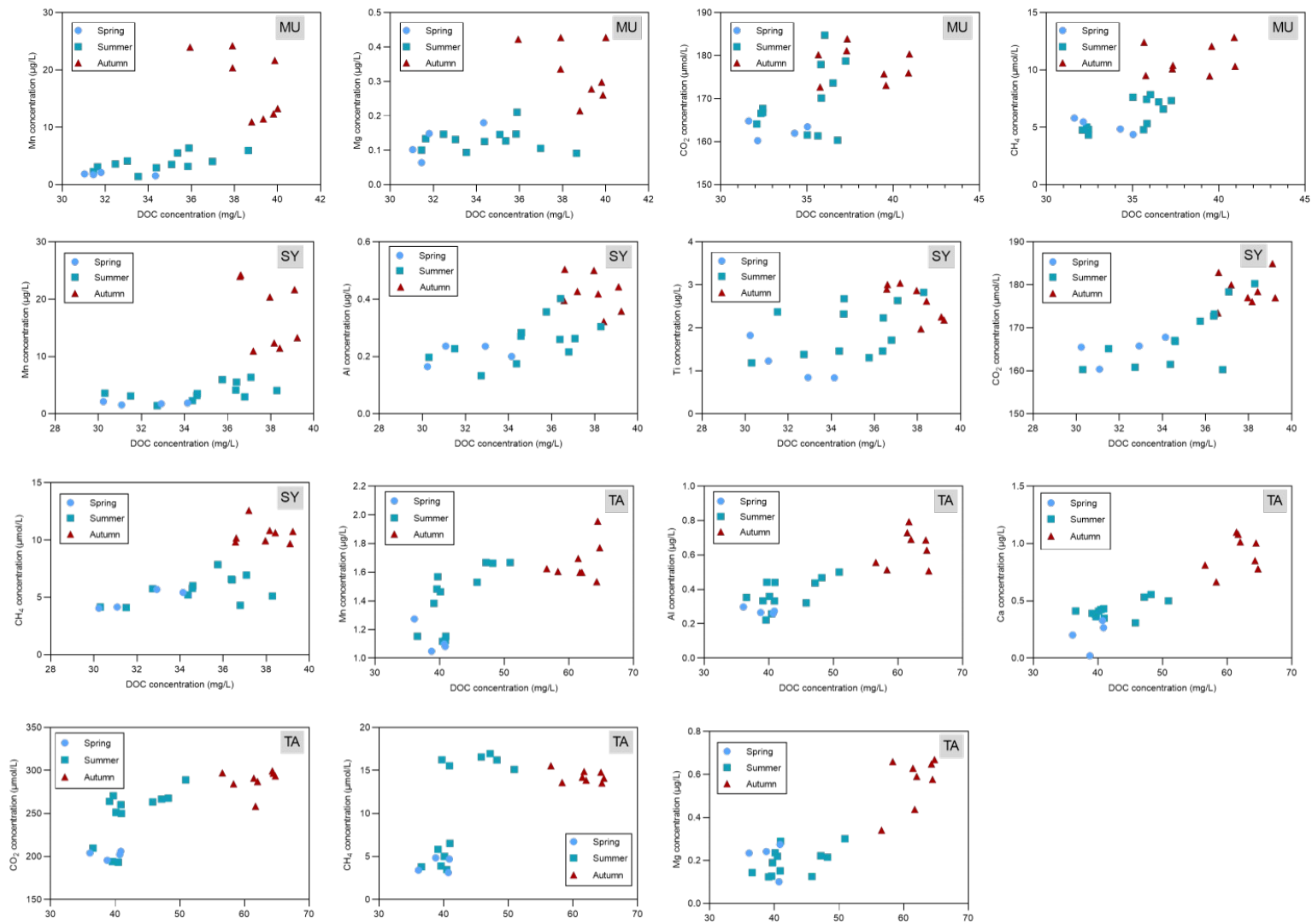
864

865 **Figure 7** Plot of partition coefficients (K_d) for the soil cores from the TA, SY, and MU sites, sampled in the late September 2016
866 K_d values were calculated by the ratio of elemental concentrations (mg/kg) in the solid soil phase to the elemental

107

108

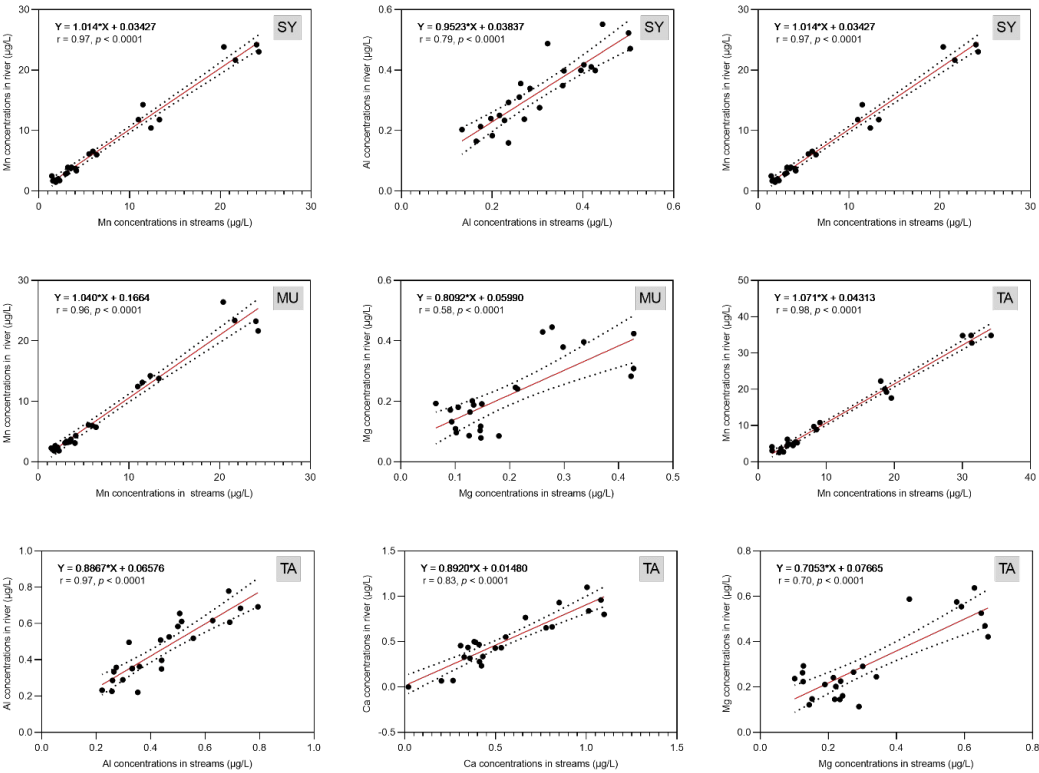
867 (m g /



869

870 **Figure 8.** Elements/ CO_2 / CH_4 -dissolved organic carbon (DOC) relationships for the
871 surrounding hydrological streams in TA, SY, and MU sites over the course of spring to
872 autumn 2016.

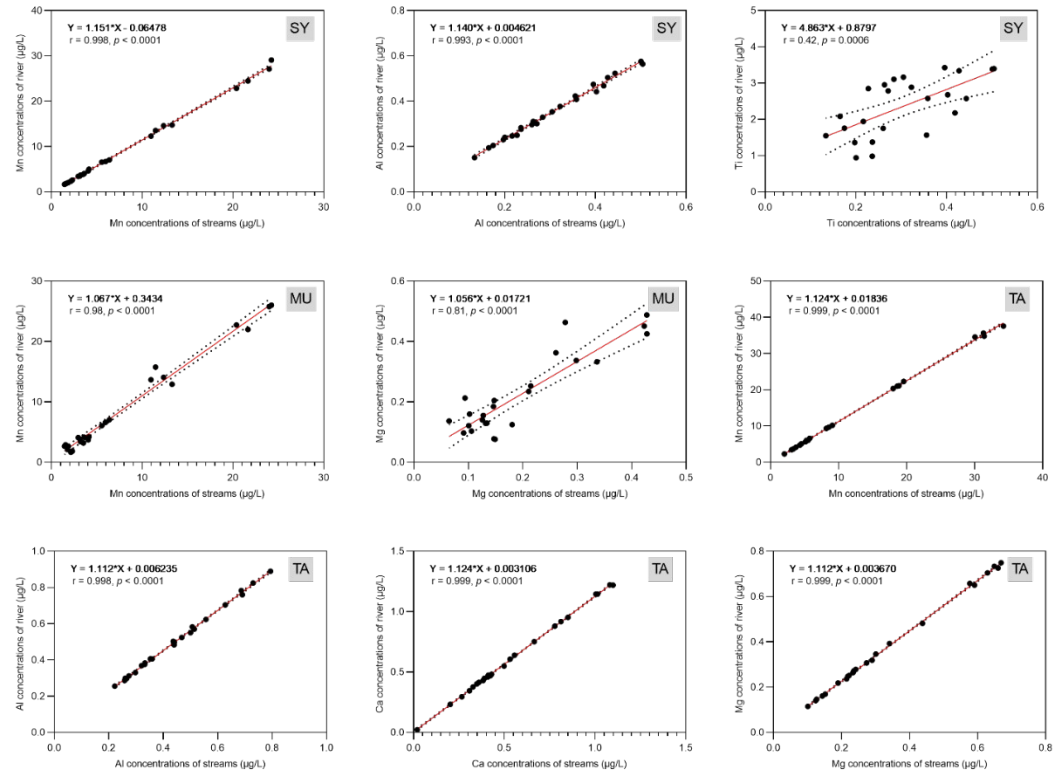
873



874

875 **Figure 9.** Linear correlations of the elements with high mobility in soil columns between the
876 connected surface streams and receiving rivers.

877



878

879 **Figure 10.** Linear correlations of the elements with high mobility in soil column between the
880 connected surface streams and supra-permafrost water.